Est. 1984

Synthesis, Characterization, and Catalytic Performance of La$_{1-x}$Ce$_x$Ni$_{1-y}$Zr$_y$O$_3$ Perovskite Nanocatalysts in Dry Reforming of Methane

PARASTOO DEZVAREHA[2], HAMIDREZA AGHABOZORGB*[1,2],
MOAYAD HOSSAINI SADRC[2] and KARIM ZARED[2]

[1,2]Department of Chemistry, Science and Research Branch, Islamic Azad University, Tehran, Iran.
[2]Research Institute of Petroleum Industry, Tehran, Iran.
*Corresponding author E-mail: dezvarehparastoo38@gmail.com

ABSTRACT

La$_{1-x}$Ce$_x$Ni$_{1-y}$Zr$_y$O$_3$ perovskite nanocatalysts were prepared by a method called citrate sol-gel. The samples were studied by the methods as X-ray diffraction (XRD), temperature programmed reduction (TPR), and inductively coupled plasma (ICP) technique.The BET method was used to determine the specific surface area. In addition, scanning and transmission electron microscopy techniques were employed to study the morphology of the prepared samples[31]. The XRD patterns confirmed the formation of perovskite with well-crystallized structure in doping level up to x= 0.1 and y= 0.2. The results of morphology studies revealed that homogenous particles in nanometer range were achieved. Based on the TPR analysis, reduction process occurred at higher temperatures and became difficult as the doping level of Zr increases. The catalytic performance was studied in dry reforming of methane (DRM) with CO$_2$. The catalyst La$_{0.9}$Ce$_{0.1}$Ni$_{0.8}$Zr$_{0.2}$O$_3$ perovskite provides the highest catalytic performance. CH4 conversion was more than 60%, CO$_2$ conversion was more than70% and the H2/CO molar ratio was ~1, respectively. Catalytic activity of La$_{1-x}$Ce$_x$Ni$_{1-y}$Zr$_y$O$_3$ nanocatalysts was enhanced when the doping level of Zr (y) increased up to 0.2, and the following result was obtained for H2/CO ratio:

LaNiO$_3$ > La$_{0.9}$Ce$_{0.1}$Ni$_{0.8}$Zr$_{0.2}$O$_3$ > La$_{0.9}$Ce$_{0.1}$Ni$_{0.9}$Zr$_{0.1}$O$_3$ > La$_{0.9}$Ce$_{0.1}$Ni O$_3$
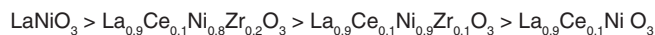
Keywords: Nanocatalyst, Catalytic performance, Perovskite, Dry reforming of methane (DRM).

INTRODUCTION

Greenhouse gases such as CO$_2$ and CH$_4$ cause global warming that is one of the greatest problem worldwide. There are many researches based on CO$_2$ consuming and H$_2$ production in order to solve the global warming such as dry reforming of methane (DRM)[1-3]. Methane dry reforming applies greenhouse gases including CH$_4$ and CO$_2$ to produce syn-gas (H$_2$+CO)[30].Syn-gas

is used in Fischer–Tropsch synthesis method to generate different chemicals[4-8]. Many of perovskite oxides behave as catalysts in the production of syn-gas regarding their stability[9-12]. ABO_3 formula of perovskites contains lanthanides, alkali metals, and alkali earth metals as A-site and transition metals are inserted in the B-site[15]. The active site in the perovskite oxide is the B-site, while the stability of the perovskite is affected by the A-site metal. The proper interaction of A and B-site metals increases the catalytic performance[13,14,16]. The dry reforming of methane employs carbon dioxide (as an oxidant) and methane on the surface of Ni-based perovskites which are resistant to coking[15]. The reactions that can occur in the dry reforming of methane are endothermic as below[33]:

$$CH_4 + CO_2 \leftrightarrow 2CO + 2H_2 \qquad \Delta H_{298k} = 247 kJ/mol \quad (1)$$

$$CO_2 + H_2 \leftrightarrow H_2O + CO \qquad \Delta H_{298k} = 41 \ kJ/mol \quad (2)$$

Partially substituting at A and B sites, affects the stability, structural defect formation, oxygen mobility in crystal lattice[34], oxygen storage, coke resistance, and catalytic activity[35,38,42]. Some examples of La substitution in $La_{1-x}M_xNiO_3$ that promotes catalytic performance are M=Ce[15-17] and Sr[18]. Resulting compounds are resistant to deposition of carbon because of numerous oxygen vacancies and presence of Ni crystallite size. Catalysts that are Ce- substituted improve catalytic behavior because they have sufficient capacity of oxygen storage and high mobility of lattice oxygen[16]. Based on Sutthiumporn *et al.,*[18] researches, B-site substitution leads to better catalytic performance and structural stability. Gallego *et al.,* studied $La_{1-x}A_xNiO_{3-\delta}$ perovskite, in which lanthanum was substituted by cerium and praseodymium, and investigated its catalytic performance and coke resistance in DRM[2]. Jahangiri *et al.,*[19-20] investigated the performance of perovskite-type oxides $La_{1-x}Sm_xNiO_3$ and $LaNi_{1-x}Fe_xO_3$ in combined reforming of methane (CRM) by changing the substitution degrees (x). Goldwasser *et al.,*[21] studied the partial substitution influence of Ru by Ni and La by Ca in $LaRuO_3$ and $LaRu_{0.8}Ni_{0.2}O_3$, respectively in CRM and DRM processes. Structural defects of the perovskite oxides can be formed by doping different metallic elements at A or B sites to increase its catalytic activity. The reduction of the metal on B site leads

to the activation of these oxide systems. The reducing process should take place on the catalyst bed[15]. Variable chemical methods such as sol-gel, co-precipitation, hydrothermal, and aerosol are applied to produce nano-sized perovskites. In the present research, $La_{1-x}Ce_xNi_{1-y}Zr_yO_3$ perovskites with various doping level up to x= 0.1 and y= 0.3 were obtained. The catalytic behavior was evaluated in DRM[30].

EXPERIMENTAL

Preparation of catalysts

$La_{1-x}Ce_xNi_{1-y}Zr_yO_3$ samples have been synthesized by a method called citrate sol-gel. Stoichiometric amounts of the cations at A and B sites were applied. $La(NO_3)_3.6H_2O$ (Merck & Co., >99/9%), $Ce(NO_3)_3.6H_2O$ (Merck & Co., >99%), $Ni(NO_3)_2.6H_2O$ (Merck & CO., >99%),[32] $ZrO(NO_3)_2.6H_2O$, (Aldrich, 99/99%)[43], ethylene glycol (99%), and citric acid (Merck & Co., 99/5%) were used[30,41]. A solution (1M) consisting of proper stoichiometric amounts of lanthanum, cerium, nickel nitrates, and zirconium oxynitrate were prepared and stirred for 40 min. at 60 °C[30]. The ethylene glycol and citric acid (1M) were added. The sol forming started and the extra water evaporated during 8 h at 80 °C[30]. The sol transformed to an amorphous spongy gel. The gel was dried for 24 h at 110 °C and calcined within 2 h at 800 °C. The rate of heating was 1°C/min. as it reached 350 °C and 3 °C/min. until it reached 800 °C.

Characterization techniques

In order to determine the crystallite structure, purity of phase and the size of the particle, X-ray patterns were studied. A 3003 PTS diffractometer, prepared the X-ray diffraction patterns of the synthesized samples[37]. The copper anode was applied in this equipment[20]. The observed X-ray patterns of the catalyst were compared with the JCPDS database that leads to identification of the phases[40]. Scanning electron microscopy (SEM) was used to study the morphology of the catalysts by employing a Philips XL30 microscope and transmission electron microscopy (TEM) applying Philips CM200 FEG microscope[30]. Temperature-programmed reduction (TPR) is a technique for determination of reduction properties of the samples. In this technique semi-automatic micrometrics TPD/

TPR 29000 apparatus was applied[30]. Based on the BET method, a Tristar 3000 Micrometrics was employed to measure the specific surface areas of the samples. In this method, N_2 at 200°C was used. Inductively coupled plasma (ICP) emission spectroscopy, measured the quantitative analysis of metals[30].

Measuring catalytic activity

The experimental studies and evaluation tests of the catalytic activity were carried out in a micro-reactor applying highly pured feed gases (CH_4, CO_2, N_2 and H_2)[20]. Controllers of the mass flow were Brooks Instrument, Model 5850. Two thermocouples and PID thermo-controllers measured and controlled the temperature of micro-reactor. 0.4 g of the catalyst was loaded in the reactor for all case studies. The flow rate of feed gases was 100 mL/min. (WHSV = 15 L/(h.g), CH_4/CO_2=1/1) under atmospheric pressure[30]. The temperature was between 600°C and 800 °C[36]. A gas chromatograph analyzed the products and reactants with FID and TCD detectors. Before measuring the activity of catalysts, the precursors should be reduced to produce the metal phase in a mixture of 20% H_2/N_2 for 2 h at 700°C. The rate of flow should be 50 mL/min.[30]. In all tests, the performance of the catalysts were evaluated by conversions. Conversions of CH_4 and CO_2, yields of H_2 and CO, and H_2/CO ratios based on the endothermic reactions attributed to this process were defined as follow[10,39]

$$CH_4 \text{ Conversion (\%)} = \frac{CH_{4,in} - CH_{4,out}}{CH_{4,in}} \times 100 \qquad (3)$$

$$CO_2 \text{ Conversion (\%)} = \frac{CO_{2,in} - CO_{2,out}}{CO_{2,in}} \times 100 \qquad (4)$$

$$\text{Yield of } H_2 \text{ (\%)} = \frac{H_{2,out}}{CH_{4,in}} \times 100 \qquad (5)$$

$$\text{Yield of CO (\%)} = \frac{CO_{out}}{CH_{4,in}} \times 100 \qquad (6)$$

$$\frac{H_2}{CO} \text{ ratio} = \frac{\text{moles of } H_2 \text{ produced}}{\text{moles of CO in feed}} \qquad (7)$$

RESULTS AND DISCUSSIONS

**Characterization of the $La_{1-x}Ce_xNi_{1-y}Zr_yO_3$ samples Crystalline structure**

The XRD patterns of the $La_{1-x}Ce_xNiO_3$ samples for x up to 0.2 and y= 0.0 are shown in Fig. 1. In the case of the Ce & Zr-free sample (x= 0.0 and y= 0.0), diffraction lines belong to the LaNiO_3 perovskite phase based on (JCPDS No.: 88-633)[15,30]. For doping level of x= 0.1 and y= 0.0, detailed examination of this pattern also revealed the perovskite phase of $La_{0.9}Ce_{0.1}NiO_3$. For substitution degree of x= 0.2, the diffraction lines of XRD pattern are characteristic of the perovskite, and also NiO and CeO_2 oxides[15]. The XRD patterns of the synthesized $La_{0.9}Ce_{0.1}Ni_{1-y}Zr_yO_3$ are seen in Fig. 2. The XRD patterns of these samples confirm that Zr doping level (y) up to 0.2 have led to the formation of mono phase and well-crystallized perovskite structure. Beyond y= 0.2, additional peaks are appeared which belong to CeO_2, NiO, and $La_2Zr_2O_7$ oxides.
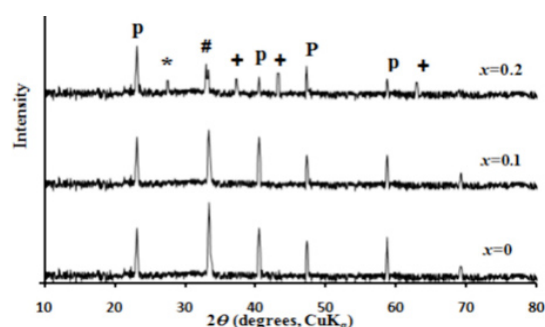
p Perovskite (JCPDS No.: 88-833)
+ NiO (JCPDS No.: 22-1189)
 # La_2NiO_4 (JCPDS No.: 83-1164) * CeO_2
(JCPDS No.: 44-1001)

Fig. 1. XRD patterns of $La_{1-x}Ce_xNiO_3$ nanocatalysts
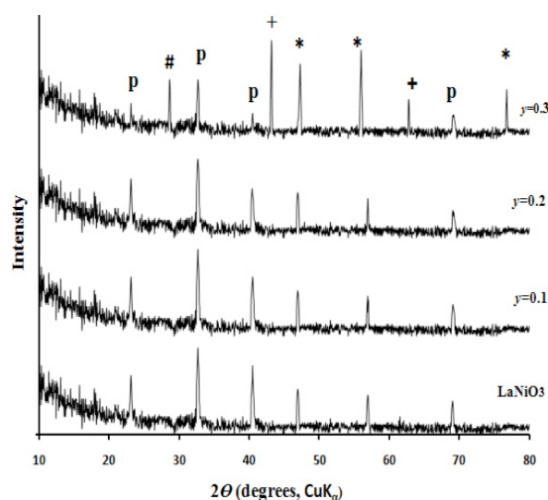
* CeO_2 (JCPDS No.: 2-1306)
#$La_2Zr_2O_7$ (JCPDS No.: 50-837)
+ NiO (JCPDS No.: 4-835)
ᵖPerovskite (JCPDS No.: 88-633)

Fig. 2. XRD patterns of $La_{0.9}Ce_{0.1}Ni_{1-y}Zr_yO_3$ nanocatalysts

Chemical analysis and surface area measurement

Table 1 shows the surface area and chemical composition (wt.%) for synthesized samples. The experimental data and the nominal value are close to each other for La, Ce, Ni, Zr (wt.%) based on ICP technique[30]. The reported values in parenthesis are nominal values. The results determine that a proper method was applied in this research. Surface areas of the catalysts based on BET method are in the range of 3-6 $m^2 g^{-1}$. Low surface area solids are the result of high temperatures exposure for long time. Scherrer equation was applied by employing the intense peak to determine the crystallite size of the obtained samples. The samples contain particles of the size in nanometers as the results confirmed.

Table 1: Crystallite size, surface areas, and elemental analysis of some $La_{1-x}Ce_xNi_{1-y}Zr_yO_3$ perovskites (calculated by Scherrer equation)

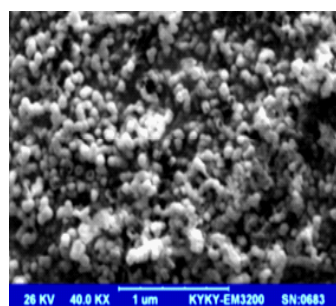| $La_{1-x}Ce_xNi_{1-y}Zr_yO_3$							
X	y	La (wt.%)*	Ce (wt.%)	Ni (wt.%)	Zr (wt.%)	SA (m^2/g)	D (nm)
0	0	69.8 (70.2)	0.0 (0.0)	30.2 (29.8)	0.0 (0.0)	6	51
0.1	0.1	62.2 (62.5)	7.0 (6.8)	26.3 (26.5)	4.5 (4.2)	3	45
0.1	0.2	61.2 (61.4)	6.9 (6.8)	23.0 (23.1)	8.9 (8.7)	5	43

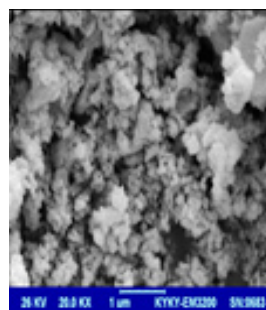* Nominal values in parenthesis

Morphology

Morphology studies of the perovskites were accomplished by SEM and TEM techniques. Figs. 3 and 4 (SEM and TEM images), reveal a uniform texture of spherical particles. The particle sizes are in nanoscale which is in consistent with crystallite sizes that calculated by Scherrer equation (see Table 2).
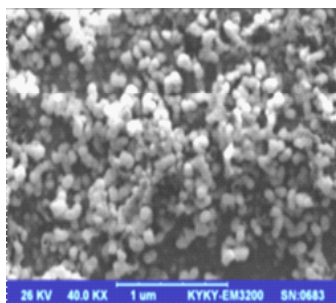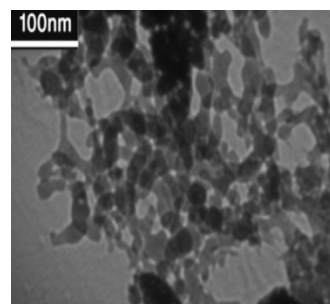

(A)

(B)

(C)

Fig. 3. SEM images of $La_{0.9}Ce_{0.1}Ni_{1-y}Zr_yO_3$ ((y = 0.1) (A), (y = 0.2) (B), (y = 0.3) (C)).

Fig. 4. TEM image of $La_{0.9}Ce_{0.1}Ni_{0.8}Zr_{0.2}O_3$ perovskite

Reducibility study of $La_{1-x}Ce_xNi_{1-y}Zr_yO_3$

Since active sites for the reforming reaction in $La_{1-x}Ce_xNi_{1-y}Zr_yO_3$ samples are nickel and zirconium, the samples have to be reduced in

order to be activated prior to the reaction. After the reduction process, Ni and Zr highly scattered on a matrix of La–Ce–O and the metal catalyst was produced. Therefore, temperature-programmed reduction is applied to study the reducibility of $La_{1-x}Ce_xNi_{1-y}Zr_yO_3$, (Fig. 5). The reduction of $LaNiO_3$ perovskite occurs in two steps. The maximum points of the peaks were apparent at 408 and 505 °C[22-23]. The first peak can be assigned to reducing of Ni^{3+} to Ni^{2+} that corresponds to $La_2Ni_2O_5$ forming[15]. The second peak can be attributed to reduction of Ni^{2+} to NiO. Cerium doped perovskites $(La_{1-x}Ce_xNiO_3)$, show slight shift to lower temperatures in TPR profile[2]. It has been reported[24] that, the reduction becomes easier while the energy of metal-oxygen bond[2,15,24] decreases. In this case study, for $La_{0.9}Ce_{0.1}NiO_3$ sample, by decreasing the ionic radius

in A-site from 103.2 pm (La^{3+}) to 101 pm (Ce^{3+}), metal–oxygen bond energy has been decreased[2]. Thus, the ease of reduction is achieved. With doping Zr into the perovskite samples ($La_{0.9}Ce_{0.1}Ni_{1-y}Zr_yO_3$), the reduction is occurred in four steps. The peaks at lower and higher temperatures can be attributed to reducing of Ni^{3+} to Ni^{2+} and Zr^{2+} to ZrO, respectively[20]. The broad peak at intermediate can be allocated to reducing of Ni^{2+} to NiO and Zr^{4+} to Zr^{2+} in the perovskite structure[25-26]. In other words, the partial replacement of nickel by zirconium in the perovskite structure made the metal reduction more difficult and the maximum of the peaks shifted to higher temperatures. Since Zr ion is more resistant to reduction than Ni ion in the ABO_3 perovskite, the Zr ions would be reduced at higher temperatures[18].
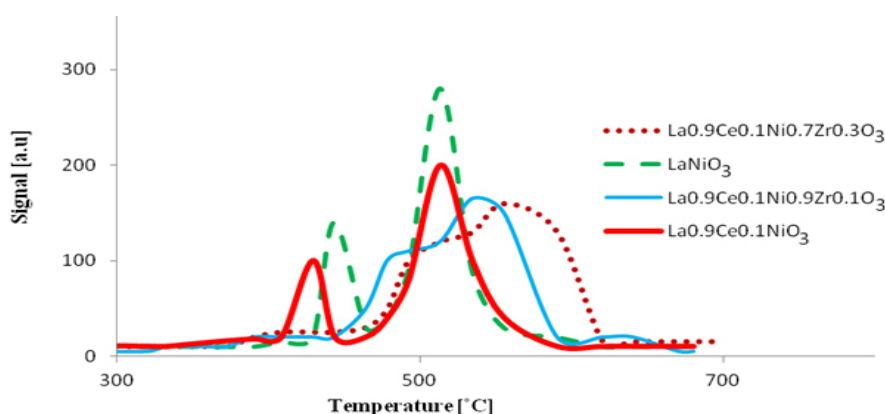

Fig. 5. TPR profiles of prepared $La_{0.9}Ce_{0.1}Ni_{1-y}ZryO_3$ calcined in air at 800 °C

Catalytic activity

Catalytic behavior of the obtained compounds has been considered for DRM process. The temperature was between 600 to 800 °C[38]. The CH_4 & CO_2 conversions and H_2 & CO yields in various temperatures, in the presence of $La_{0.9}Ce_{0.1}Ni_{1-y}Zr_yO_3$ are prepared in Fig. 6. CH_4 and CO_2 conversions grow by rising the temperature. The conversions of CO_2 are higher than that of CH_4. It can be the result of CO_2 consuming in reaction equations 1 and 2. Consequently, by rising reaction temperature, both H_2 and CO yields increase and the CO yields are higher than that of H_2. This feature is more notable at higher temperatures. In reactions with $La_{0.9}Ce_{0.1}Ni_{1-y}Zr_yO_3$ catalyst that the partial doping level is y= 0.3, there is not notable product yields at any temperature. H_2/CO ratio is ~1, in the reactions

containing $La_{0.9}Ce_{0.1}Ni_{1-y}Zr_yO_3$ with doping level of y=0.1 and y=0.2. It can be concluded that the reaction equation 1 may be the main reaction[30]. Based on these results, mono phase perovskites are proper to produce more H_2. H_2/CO ratio is less than 1 where Zr doping level of the applied catalyst is y>0.2 and has more than one phase. In samples without Zr ($La_{0.9}Ce_{0.1}NiO_3$) this ratio is also less than 1. In Fig. 7 the CH_4 & CO_2 conversions, and H_2 & CO yields versus time for $La_{0.9}Ce_{0.1}Ni_{1-y}Zr_yO_3$ samples are presented. These diagrams reveal that in reactions containing the pure perovskite, CH_4 & CO_2 conversions and H_2 & CO yields are higher in comparison with reactions containing more than one phase. In reactions containing $La_{0.9}Ce_{0.1}Ni_{0.8}Zr_{0.2}O_3$ catalyst the H_2/CO ratio is ~1 with the best catalytic performance (Fig. 8). In reactions containing

$La_{1-x}Ce_xNi_{1-y}Zr_yO_3$ samples, the content of Ce and Zr control the CH_4 and CO_2 conversions in DRM process. Redox chemistry, heat stability, ionic conductivity and the oxygen transporting capability of Zr is notable in proper catalytic behavior of these nanocatalysts[27-29]. High redoxability of cerium upgrades the catalytic characteristic of Ni-based catalysts[2] in DRM[30].
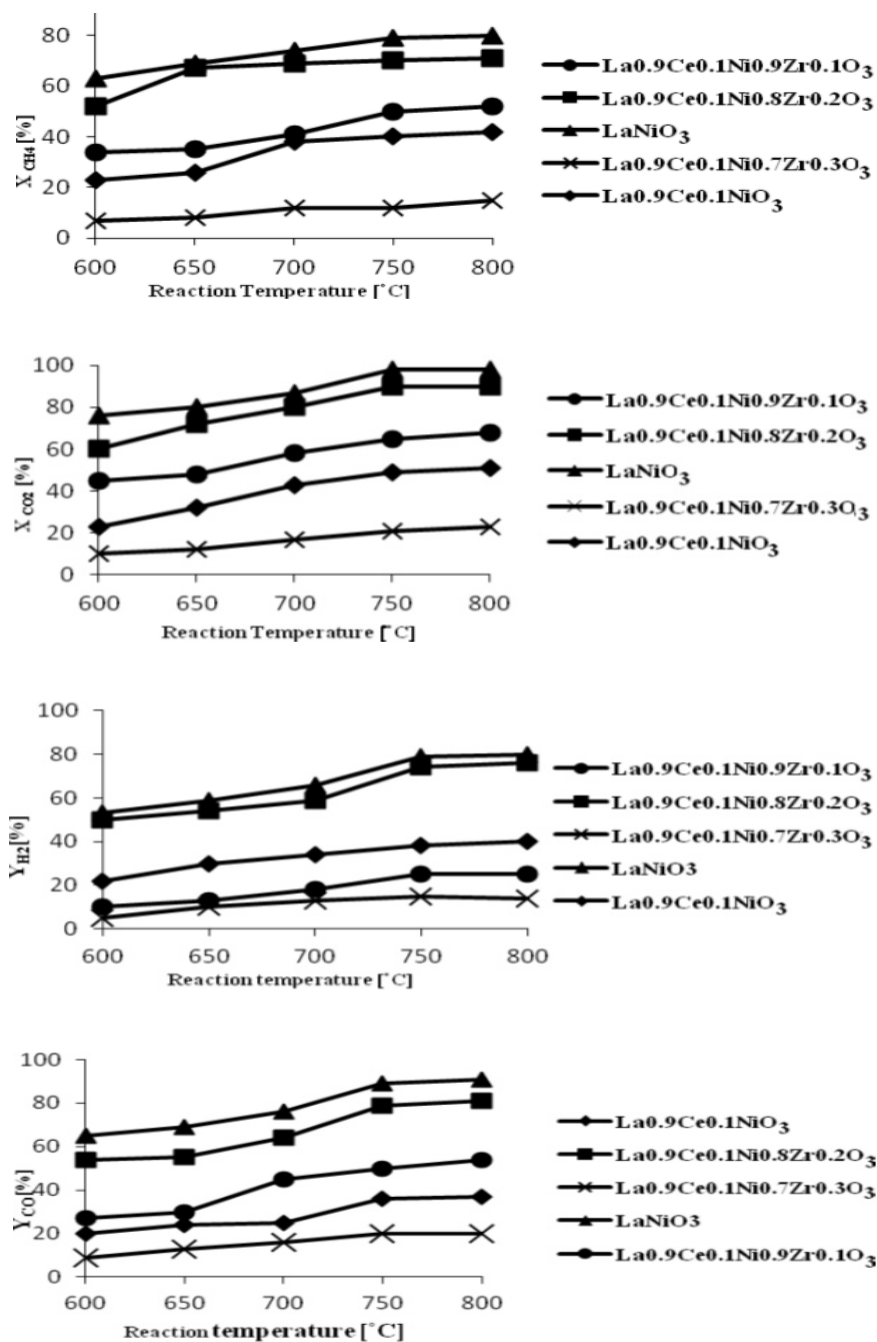

Fig. 6 Conversions of CH$_4$ and CO$_2$, and H$_2$ and CO yields versus temperature for La$_{0.9}$Ce$_{0.1}$Ni$_{1-y}$Zr$_y$O$_3$ samples in DRM process (CH$_4$/CO$_2$= 1/1 and WHSV=15L/(h.g)).
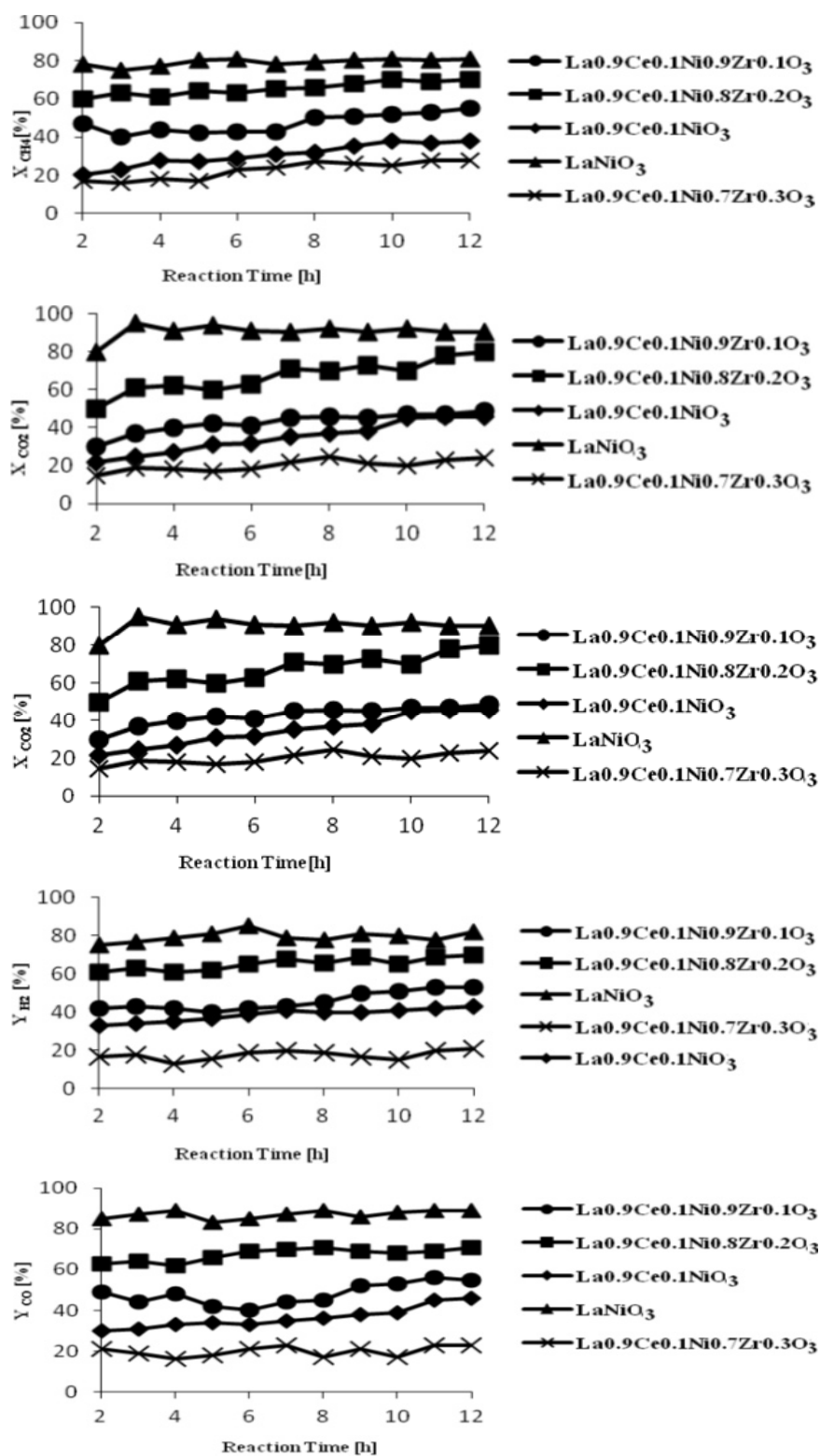
Fig. 7. Conversions of CH_4 and CO_2, H_2 and CO yields versus time for $La_{0.9}Ce_{0.1}Ni_{1-y}Zr_yO_3$ samples at 750 °C in DRM process (CH_4/CO_2= 1/1 WHSV=15L/(h.g)).
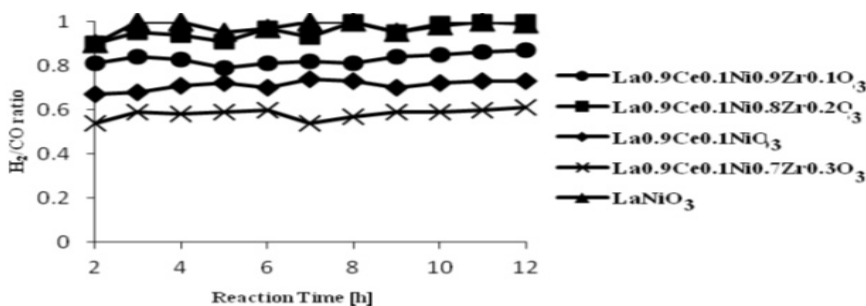
Fig. 8. H$_2$/CO ratios for La$_{1-x}$Ce$_x$Ni$_{1-y}$Zr$_y$O$_3$ versus time in DRM process (CH$_4$/CO$_2$= 1/1 WHSV=15L/(h.g))

CONCLUSION

1. The perovskite La$_{1-x}$Ce$_x$Ni$_{1-y}$Zr$_y$O$_3$ (x=0.1, y=0.1, 0.2) nanocatalysts were prepared by a method called citrate sol-gel. Spherical particles on a nanometer scale were produced.

2. Based on TPR analysis, partial substitution of Ni by Zr in La$_{0.9}$Ce$_{0.1}$Ni$_{1-y}$Zr$_y$O$_3$ perovskite led to a difficult reducibility of nickel, and consequently, the metal reduction shift to higher temperatures.

3. By rising the temperature, CH$_4$ & CO$_2$ conversions and the yields of H$_2$ & CO increased, while the pure perovskite was present in the reaction.

4. Partially substituted perovskite La$_{0.9}$Ce$_{0.1}$Ni$_{0.8}$Zr$_{0.2}$O$_3$ performed the best catalytic activity.

REFERENCES

1. Valderramaa, G.; Kiennemannb, A.; Goldwasser, M. R. Power Sources., **2010**, *195*, 1765-1771.

2. Gallego German, S.; Marin Jaime, G.; Batiot-Dupeyrat, C.; Barrault, J.; Mondragon, F.; *Appl. Catal. A: Gen.*, **2009**, *369*, 97-103.

3. Steinhauer, B.; Kasireddy, M.R.; Radnik, J.; Martin, A. *Appl. Catal. A: Gen.*, **2009**, *366*, 333-341.

4. Bedel, L.; Roger, A. C.; Estournes, C.; Kiennemann, A.; *Catal. Today.*, **2003**, *85*, 207-218.

5. Zhang, W. D.; Liu, B. S.; Zhu, C.; Tian, Y. L.; *Appl. Catal. A: Gen.*, **2005**, *292*, 138-143.

6. Ruckenstein, E.; Wang, H. Y. *Catal, Lett.*, **2001**, *73*, 99-105.

7. Eltejaei, H.; Bozorgzadeh, H. R.; Towfighi, J.; Omidkhah, M. R.; Rzari, M.; R. Zanganeh, R. *Int. J. Hydrogen Energy.*, **2012**, *37*, 4107-4118.

8. García-Diéguez, M.; Pieta, I. S.; Herrera, M. C.; Larrubia, M. A.; Alemany, L. J. *J. Catal.* **2010**., *270*, 136–145.

9. Urasaki, K.; Tokunaga, K.; Sekine, Y.; Matsukata, M.; Kikuchi, E. *Catal. Commun.*, **2008**, *9*, 600-601.

10. Dejaidja, A.; Libs, S.; Kiennemann, A.; Barama, A.; *Catal. Today.,* **2006**, *113*, 194-200.

11. Gallego, G. S.; Mondragon, F.; Barrault, J.; Tatibouet, J. M.; Dupeyrat, C. B. *Appl. Catal A: Gen.,* **2006**, *311*, 164-71.

12. Mawdsley, J. R.; Krause, T. R. *Appl. Catal.*, **2008**, *334*, 311-312.

13. Chendong, Z.; Doris, S.; Balachandran, U.; Meilin, L. *Chem. Mater.*, **2006**, *18*, 4647-4650.

14. Pereniguez, R.; Gonzalez-Dela Cruz, V. M.; Holgado, J. P.; A. Caballero, *Appl. Catal.*, **2010**, *93*, 346-353.

15. Lima, S. M.; Assaf, J. M.; Pena, M. A.; Fierro, J. L. G. *Appl. Catal.*, **2006**, *311*, 94-104.

16. Choi, S.; Moon, S. H. *Catal. Today.*, **2009**, *146*, 148-153.

17. Lima, S. M.; Silva, A. M.; Costa, L. O. O.; Assaf, J. M.; Mattos, L. V.; Sarkari, R. *Appl. Catal. B.*, **2012**, *121*, 1-9.

18. Sutthiumporn, K.; Maneerung, T.; Kathiraser, Y.; Kawi, S. *Int. J. Hydrogen Energy.*, **2012**, *37*, 11195-11207.

19. Jahangiri, A.; Aghabozorg, H. R.; Pahlavanzadeh, H. *Int. J. Hydrogen Energy.*, **2013**, *38*, 10407-10416.

20. Jahangiri, A.; Pahlavanzadeh, H.; Aghabozorg,

H. R. *Int. J. Hydrogen Energy.*, **2012**, *37*, 9977-9984.

21. Goldwasser, M. R.; Rivas, M. E.; Pietri, E.; Perez-Zurita, M. S.; Cubeiro, M. L.; Gingembre, L.; Leclercq, L.; Leclercq, *G. Appl. Catal.*, **2003**, *225*, 45-47.

22. Jahangiri, A.; Aghabozorg, H.R.; Pahlavanzadeh, H.; J, Tow fighi, J. *Int. J. Chem. React. Eng.*, **2014**, *12*, 1–10.

23. Valderrama, G.; Kiennemann, A.; Goldwasser, M. R. *Catal. Today.*, **2008**, *133*, 142–148.

24. Catherine, B. D.; Gallego, G. A. S.; Mondragon, F.; Barrault, J.; Tatibouet, J. M. *Catal. Today.*, **2005**, *107*, 474-480.

25. Zhongshan, Y.; Changjun, N.; Chunxi, Z.; Diannan, G.; Shudong, W.; Yuming, X.; Akira, O. *Catal. Today.*, **2009**, *146*, 124–131.

26. Jun, K.W.; Roh, H.S.; Chary, K.V. *Catal. Surv. Asia.*, **2007**, *11*, 97–113.

27. Valderrmaa, G.; Goldwasser, M. R.; Navarro, C. U.; Tatibouët, J. M.; Barrault, J.; Dupeyrat, C. B.; Martinez, F. *Catal. Today.*, **2005**, *107*, 785–791.

28. Supaporn, T.; Apichai, T.; Chairut, S.; Sarayut, Y. *Int. J. Hydrogen Energy.*, **2008**, *33*, 991-999.

29. Choque, V.; Ramírez, P.; Molyneux, D.; Homs, N. *Catal. Today.*, **2010**, *149*, 248–253.

30. Talaie, N.; Hossaini Sadr, M.; Aghabozorg, H.R.; Zare, K. *Orient. J. Chem.*, **2016**, *32* (5). 304-315.

31. Pakhare, D.; Schwartz, V.; Abdelsayed, V.; Haynes, D.; Shekhawat, D.; Poston, J.; Spivey, J. *J.Catal.*, **2014**, *316*, 78-92.

32. Soongprasit, K.; Aht-Ong, D.; Sricharoenchaikul, V.; Atong, D. *Current Applied Physics.*, **2012**, *12*(2), 80-88.

33. Lim, H. S.; Kang, D.; Lee, J. W. Appl. Catal. B: *Invironmental.*, **2017**, *202*, 175-183.

34. Pakhare, D.; Spivey, *J., Chem. Soc. Rev.*, **2014**, *43*, 7813-7837.

35. Bushra, I.; Syed Tajammul, H.; Sohaib, A. *Chem. Ing. J.*, **2013**, *219*, 395-402.

36. Lucrédio, A. F.; Assaf, J.M.; Assaf, E. M. *Appl. Catal. A: Gen.*, **2011**, *400*, 156-165.

37. Barros, B.S.; Libs, S.; Melo, D. M. A.; Kiennemann, A. *Appl. Catal. A: Gen.*, **2010**, *378*(1), 69-75.

38. Li, J.; Li, J. G.; Zhang, Z.; Wu, X.; Liu, S.; Li, X.; Sun, X.; Sakka, Y. *Sci. Technol. Adv. Mater.*, **2012**, *13*(3),235-250.

39. Liu, B.S.; Zgao, L.; Au, C.T. *Appl. Catal. A: Gen.*, **2002**, *235*, 193-206.

40. Kwak, J. H.; Lee, S. G.; Lee, S. H.; Park,Y. K.; Sohn, *J. M. Catal. Today.*, **2014**, *232*, 11-15.

41. Logvinovich, D.; Sheptyakov, D.; Bocher, L.; weidenkaff, A. *Solid State Sciences.*, **2009**, *11*(8), 1513-1519.

42. De Caprariis, B.; De Filippis, P.; Palma, V.; Petrullo, A.; Ricca, A.; Ruocco, C.; Scarsella, M. *Appl. Catal. A: Gen.*, **2016**, *517*, 47-55.

43. Mohebbi, H.; Ebadzadeh, T.; Hesari, F.A. *Powder Technology.*, **2009**, *188*, 183-186.